

Carrier-carrier correlations in an optically excited single semiconductor quantum dot

E. Dekel, D. Gershoni, and E. Ehrenfreund

Physics Department and Solid State Institute, Technion-Israel Institute of Technology, Haifa 32000, Israel

J. M. Garcia and P. M. Petroff

Materials Department, University of California, Santa Barbara, California 93106

(Received 17 March 1999; revised manuscript received 15 November 1999)

We applied low-temperature diffraction-limited confocal optical microscopy to spatially resolve and spectroscopically study photoluminescence from single self-assembled semiconductor quantum dots. Using selective wavelength imaging we unambiguously demonstrated that a single photoexcited quantum dot emits light in a few very narrow spectral lines. The measured spectrum and its dependence on the power of either cw or pulsed excitation are explained by taking carrier correlations into account. We solve numerically a many-body Hamiltonian for a model quantum dot, and we show that the multiline emission spectrum is due to optical transitions between confined exciton multiplexes. We furthermore show that the electron-electron and hole-hole exchange interaction is responsible for the typical appearance of pairs in the photoluminescence spectra and for the appearance of redshifted new lines as the excitation power increases. The fact that only a few spectral lines appear in the emission spectrum strongly indicates fast thermalization. This means that a multi-exciton relaxes to its ground state much faster than its radiative lifetime.

I. INTRODUCTION

The study of electronic properties of the semiconductor heterostructure of reduced dimensionality has been a subject of many recent extensive efforts. These efforts are motivated both by their potential device applications as well as by their being an excellent stage for experimental studies of basic quantum mechanical principles. Semiconductor quantum dots (QD's) of nanometer size are of particular interest since carriers are confined there within dimensions smaller than their de Broglie wavelength. This confinement in three directions results in a characteristic discrete energy spectrum and a δ -like density of states.¹

One of the simplest and therefore most common ways of producing semiconductor QD's is the Stranski and Krastanov self-assembled growth of strained QD's (SAQD's).²⁻⁴ In this growth mode, the elastic energy associated with the lattice mismatch strain between different epitaxially deposited semiconductor layers is minimized through the formation of small islands connected by a thin wetting layer.⁵ These high crystalline quality islands are typically of pyramidal shape of 10–30 nm base dimensions and 2–8 nm height.⁶ By capping these self-assembled islands with an epitaxial layer of wider band-gap material and a lattice constant that is similar to that of the substrate, high-quality QD's are produced. One of the main disadvantages of this growth mode is the size distribution of the SAQD's, which is typically about $\pm 10\%$. This, together with possible distributions in composition, strain field, and structural shape, gives rise to a large nonuniformity of the SAQD properties in general and inhomogeneous broadening of their optical spectral features in particular.^{1,3-7} This has been a long-standing impediment on the studies of SAQD's, which has so far limited the ability to correctly interpret and clearly understand the experimental data. An obvious way to overcome this obstacle is to optically study a single quantum dot.⁸⁻¹¹ By doing so one can completely

avoid the inhomogeneous broadening and therefore expect to explore the energy spectrum of confined charge carriers in the QD, and the interactions and correlations among them.¹²⁻¹⁴ A typical signature of such studies is the appearance of sharp and distinct spectral lines in the low-temperature photoluminescence (PL) spectrum due to the discrete nature of the energy levels of carriers that radiatively recombine within these "zero-dimensional" QD's.^{11,15} Recently, the effects of externally applied electric and magnetic fields on such isolated quantum systems were studied by monitoring their influence on the PL spectrum.¹⁶⁻¹⁸

The presence of few confined carriers in such a small volume gives rise to correlated few carrier multiplexes,¹⁹⁻²¹ which are unstable otherwise. Therefore, the analysis of the optical studies of these systems is fundamentally different than the analysis of recombination processes in systems of higher dimensionality.

In this paper, we present continuous wave (cw) and pulsed PL spectroscopy measurements of the recombination processes in single SAQD's. For the analysis of our data we outline a theoretical model that quite systematically explains the measured PL spectra and quantitatively accounts for their dependence on the excitation power in both cw and pulsed mode. In particular, we demonstrate that the electron-electron ($e-e$) and hole-hole ($h-h$) exchange interaction energies can be directly obtained from the PL spectra. We unambiguously show, in fact, that these exchange terms are most instrumental for the understanding of the experimental results when more than two carriers of the same type participate in the radiative process.

This paper is organized as follows. In Sec. II we present our theoretical multiexciton model. In Sec. III we present the low-temperature PL spectroscopy of single SAQD's, and in Sec. IV the experimental data are discussed in terms of the model of Sec. II. Our conclusions are briefly summarized in Sec. V.

II. THE MULTIEXCITON MODEL

A. Energy levels

We describe the many-body Hamiltonian of a single QD in terms of its single carrier energies and wave functions,

$$H = H_{free}^e + H_{free}^h + H_{coul}^{e-e} + H_{coul}^{h-h}, \quad (1)$$

where

$$H_{free}^h = \sum_j \varepsilon_j b_j^\dagger b_j, \quad H_{free}^e = \sum_j \varepsilon_j a_j^\dagger a_j, \quad (2)$$

$$H_{coul}^{e-e} = \frac{1}{2} \sum_{i_1, i_2, i_3, i_4} a_{i_1}^\dagger a_{i_2}^\dagger a_{i_3} a_{i_4} G_{i_1, i_2, i_3, i_4}, \quad (3)$$

$$H_{coul}^{e-h} = - \sum_{i_1, j_2, j_3, i_4} a_{i_1}^\dagger a_{i_4} b_{j_3}^\dagger b_{j_4} G_{i_1, j_2, j_3, i_4} \\ + \sum_{j_1, i_2, j_3, i_4} a_{i_2}^\dagger a_{i_4} b_{j_3}^\dagger b_{j_1} G_{j_1, i_2, j_3, i_4}, \quad (4)$$

$$H_{coul}^{h-h} = \frac{1}{2} \sum_{j_1, j_2, j_3, j_4} b_{j_1}^\dagger b_{j_2}^\dagger b_{j_3} b_{j_4} G_{j_1, j_2, j_3, j_4}. \quad (5)$$

In Eqs. (2)–(5), a_i, b_j (a_i^\dagger, b_j^\dagger) are the annihilation (creation) operators for electrons and holes, respectively, and $\varepsilon_i, \varepsilon_j$ are their corresponding one-particle energy levels within the QD. The summation index i (j) runs over all the electron (hole) one-particle states (spin-degenerate states are included). The Coulomb interaction terms, Eqs. (3)–(5), can be expressed in terms of the one-particle (electron and hole) envelope wave functions $\phi_{l,B}(\vec{x})$ as follows:

$$G_{l_1, l_2, l_3, l_4} = \delta_{s_4, s_1} \delta_{s_3, s_2} \int \int d^3x d^3x' \phi_{l_1, B}^*(\vec{x}) \phi_{l_2, B}^*(\vec{x}') \\ \times \frac{e^2}{\varepsilon |\vec{x} - \vec{x}'|} \phi_{l_3, B}(\vec{x}') \phi_{l_4, B}(\vec{x}), \quad (6)$$

where δ_{ij} is the Kronecker delta and s_i and e are the spin and charge of the respective single carrier state, $B = C, V$ is the band index, and l_i represents the set of quantum numbers that characterizes the single carrier envelope function.

Since the main subject of this work is the optical properties of a single dot containing a few interacting carriers in it, we chose to describe the single-particle states in the simplest possible form. As shown below, a typical PL spectrum from a single quantum dot is composed of a few spectral lines. These lines result from the multicarrier occupation of the emitting dot. We show below that the spectral positions of these lines, as well as their dependence on the excitation power, can be described by two important physical properties of the dots. Namely, the single carrier energy level separation and the exchange integrals between these levels. We show that these two *most meaningful* parameters can, in fact, be accurately deduced from the measured spectrum. Furthermore, we have found out that the exchange integrals between single carrier states, the many carrier wave functions, and the oscillator strength for optical transitions between them are not strongly dependent on the details of the single carrier

wave functions. They strongly depend, however, on the symmetry and spin degeneracy of these single carrier wave functions. These are accurately given by the following very simple single carrier model. In this model both electrons and holes are described by envelope functions that are the analytical solutions of a potential structure described by a rectangular box of dimensions L_x, L_y, L_z , and infinite potential barriers,

$$\phi_{l,B}(\vec{x}) = \sqrt{\frac{2^3}{L_x L_y L_z}} \sin\left(\frac{n_x \pi}{L_x} x\right) \sin\left(\frac{n_y \pi}{L_y} y\right) \sin\left(\frac{n_z \pi}{L_z} z\right), \quad (7)$$

where n_x, n_y, n_z ($=1, 2, 3, \dots$), are the quantum numbers associated with the respective axes. We note that in this one-band simplified model the small e - h exchange interaction²² strictly vanishes.

We now diagonalize numerically the Hamiltonian (1) to yield all the multicarrier energy levels and their corresponding wave functions. Since in this work we study an undoped sample in which carriers are excited optically, we deal here only with neutral multicarrier states with an equal number of electrons and holes. We note, however, that the model is general enough to allow analysis of charged QD's as well. In order to keep the description concise, we consider in the following discussion only the lowest four single electron and four single hole energy levels. These levels, denoted hereafter by (111), (211), (121), and (221), are characterized by the quantum numbers associated with the confinement along the Cartesian axes x, y , and z , respectively. In this geometrically nonsymmetric ($L_x > L_y \gg L_z$) box, each of these single carrier states is only doubly spin ($\uparrow\downarrow$) degenerate.

1. Uncorrelated carriers

As an example, we describe in Fig. 1 a few simple cases. First, we consider the case in which only one electron-hole pair occupies the QD [Fig. 1(a)]. If the Coulomb interaction within the pair can be ignored, it is readily seen that there are 16 possible different energy levels and each one is four times degenerate due to the various electron and hole spin states [left side of Fig. 1(a), where for simplicity only four levels are shown]. We denote the four lowest energy states of the noninteracting pair by, $1e^\uparrow 1h^\uparrow$, $1e^\uparrow 1h^\downarrow$, $1e^\downarrow 1h^\uparrow$, and $1e^\downarrow 1h^\downarrow$, respectively. Here $1e(h)^\uparrow$ means one electron (hole) in its lowest single carrier level (111). Similarly, assuming that the effective mass of the hole is larger than that of the electron, the degenerate states of the second energy level are denoted by $1e^\uparrow 1h^2\uparrow$, $1e^\uparrow 1h^2\downarrow$, $1e^\downarrow 1h^2\uparrow$, and $1e^\downarrow 1h^2\downarrow$, respectively. In these states, one hole resides in its second energy level (211).

The situation in which two electrons and two holes occupy the dot can be similarly described. Here, there are altogether 784 biexciton states in 100 energy levels and, unlike the exciton energy levels, the degeneracy is energy level dependent [Fig. 1(b), where for simplicity only nine levels are shown]. There are nondegenerate levels such as the lowest biexcitonic energy level $1e^\uparrow 1e^\downarrow 1h^\uparrow 1h^\downarrow$, in which all the participating single carrier electron and hole levels are full. There are also levels of maximum of 16-fold degeneracy, like $1e^\uparrow 1e^2 1h^\uparrow 1h^2$, in which two different electron and hole levels are half full. These energy levels and a few

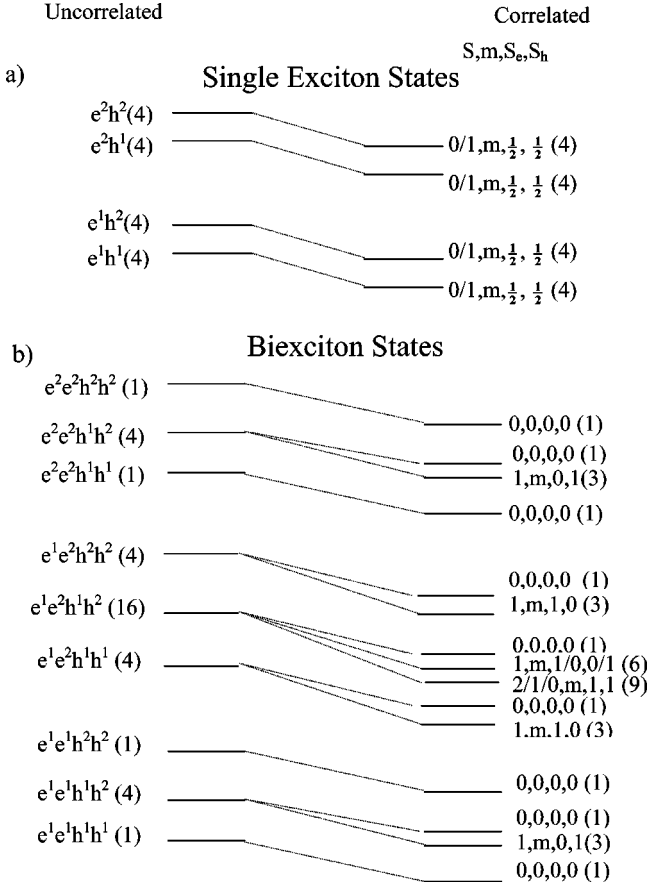


FIG. 1. Schematic description of the energy levels of the QD confined single-exciton and biexciton multiplexes. On the left (right) side of the figure the levels are described without (with) the Coulomb interaction. The numbers in parentheses represent the level degeneracy and the symbols $e^i (h^j)$ stand for electron (hole) in their i th (j th) single carrier level.

other noncorrelated ones are illustrated on the left side of Fig. 1.

2. Correlated carriers

Let us consider now the effect of the Coulomb interaction on these multicarrier states. Since the Hamiltonian is spin independent it commutes with spin operators. Therefore, their eigenvalues can be used to characterize the eigenstates of the full Hamiltonian [Eq. (1)]. The “good” quantum numbers that we introduce¹² are the total electron (hole) spin $S_{e(h)}^2$, the total spin S^2 , and its projection along the z axis, S_z . In the case of one electron-hole pair (“single exciton”), as can be seen in the right-hand side of Fig. 1, the Coulomb attraction gives rise to a rigid downward shift of all the energy levels. However, there is no degeneracy removal and all the excitonic levels remain four times degenerate. (We note here that the electron-hole exchange interaction, which we ignore, should in principle, remove the degeneracy between the three $S^2=1$ states and the one $S^2=0$ state of each energy level.²³)

The situation is vastly different for the case of two electrons and two holes (a “biexciton”). A noteworthy example is the 16-fold degenerate $1e^11e^21h^11h^2$ level. Here, the e - e and h - h exchange interactions partly remove the degeneracy

by splitting it into three levels. The lowest level with $S_e^2=1$ and $S_h^2=1$ is ninefold degenerate. The second level with $S_e^2=1(0)$ and $S_h^2=0(1)$ is sixfold degenerate. The third is a nondegenerate level, with $S_e^2=0$ and $S_h^2=0$. We demonstrate below that this spin degeneracy removal reveals itself in a characteristic multispectral line PL spectrum. We further show that such a behavior is characteristic to all even multiexciton (i.e., even number of correlated electron-hole pairs) cases.

B. Optical transitions between multiexciton states

We proceed and calculate, using the dipole approximation, the matrix elements for optical transitions between initial and final exciton multiplexes (multiexcitons), which differ by one e - h pair (exciton). Such optical transitions of e - h annihilation can occur only between states of the same S^2 and S_z eigenvalues. As discussed above for the biexciton case, there are several hundred degenerate energy levels for each N th ($N \geq 2$) multiexciton. Therefore, there are typically hundreds of allowed optical transitions of different photon energies between the $(N+1)$ th to the N th multiexciton cases.

If the radiative rate is much slower than the thermalization rate, fast thermalization to the ground multiexcitonic states will significantly lower the number of these transitions. Our experimental observation¹⁴ and others^{10,21} are definitely in accordance with the assumption that the QD is in thermal equilibrium when photons are emitted due to exciton annihilation. Therefore, in the following, we consider only optical transitions from the ground energy level of each $(N+1)$ th multiexciton to all possible levels of the N th multiexciton.

As an example, we schematically display in Fig. 2 all the allowed optical transitions that result from the radiative annihilation of a triexciton in its ground energy level. The subsequent creation of the biexciton states is also described in the figure. As can be seen, in the noncorrelated energy level scheme (Fig. 2, left side) only two optical transitions are allowed. The first is due to the recombination of electron and hole in their first one-carrier energy levels, and the second is due to the recombination of electron and hole in their second energy levels. In the correlated carrier picture, however (Fig. 2, right side) we show that the first optical transition splits into two strong and one weak distinct transitions due to the splitting of the 16 times degenerate $e^1e^2h^1h^2$ energy level as discussed above. This behavior is not limited to this optical transition only. As can be readily understood, similar splitting occurs also in every optical transition between odd to even higher multiplexes of excitons.

This splitting results directly from the exchange interaction between carriers of the same charge. Its magnitude depends on the Coulomb integral as given by Eq. (6). In Table I, we list the nonvanishing exchange integrals that involve carriers within the first two energy levels of our model rectangular QD. In these calculations L_x , L_y , and L_z were set to 30.5, 30.0, and 5.0 nm, respectively, and the InAs dielectric constant (15.0) was used.²⁴ As we discuss below, these dimensions were chosen to best fit our experimental observations. We note in Table I that the exchange integral between the pair of levels (211)-(121) and (111)-(221) is roughly half

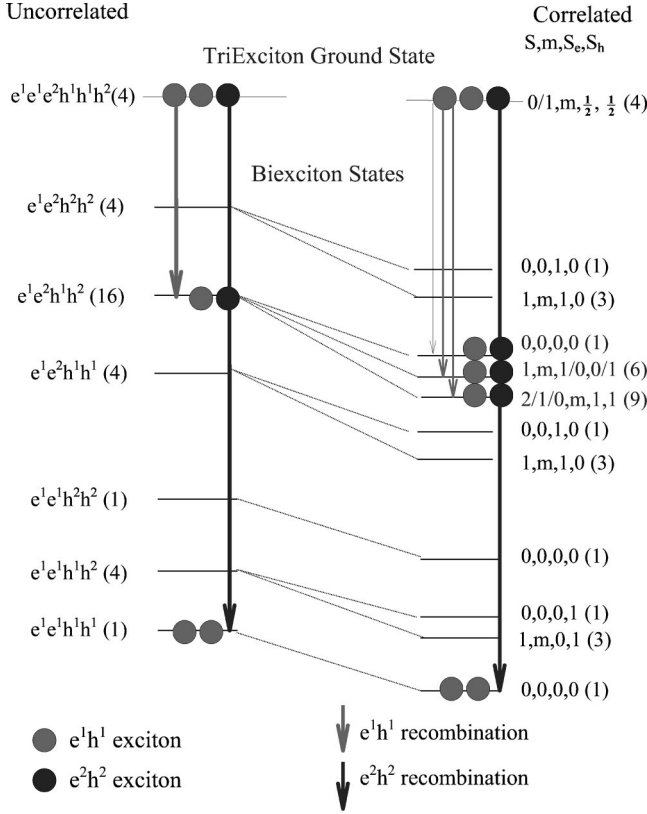


FIG. 2. Schematic description of the allowed optical transitions between the ground triexciton energy level to the biexciton states, without (left side) and with (right side) the Coulomb interaction. The light (dark) gray vertical lines represent e^1h^1 (e^2h^2) pair recombination.

the magnitude of that between (111)-(211) and (111)-(121). We will return to this point in the discussion of our experimental measurements.

The $e-e$ and $h-h$ exchange interactions are responsible for the line splitting described in Fig. 2. In addition, they give rise to a spectral redshift of optical transitions from successively higher multiplexes of excitons, as demonstrated in Fig. 3. These redshifts are caused by the number of exchange interactions, which increases with the number of carriers. Therefore, the sum of exchange interaction energies lowers the energy of the $N+1$ multiexciton levels more than it low-

TABLE I. Calculated exchange energies for confined carriers within the model quantum dot.

j	$n_x n_y n_z$	Δ_{1j} (meV)	Δ_{2j} (meV)
1	111		3.49
2	211	3.48	
3	121	3.48	1.57
4	221	1.57	2.98
5	311	2.17	2.83
6	131	2.17	1.14
7	321	1.14	1.27
8	231	1.14	1.89
9	411	1.47	1.82
10	141	1.47	0.84

ers the energy of the N multiexciton levels, thus causing successive redshifts in the transition energies.

In Fig. 3 we summarize all the calculated optical transitions resulting from the radiative annihilation of up to eight multiexciton ground states. For these calculations an InAs band gap of 0.625 eV and electron and hole effective masses of 0.023 and 0.6 electron rest mass, respectively, were used.²⁴ Here, only transitions that result from annihilation of electron and hole in their lowest two single carrier levels are considered. A thin (thick) solid arrow denotes transitions due to radiative recombination of e^1h^1 (e^2h^2) pairs. A dashed arrow denotes the recombination of e^2h^1 or e^1h^2 pairs, which becomes partially allowed due to Coulomb interaction mixing. We present only the relevant levels that participate in the radiative recombination processes of the ground multiexciton levels. Since mainly symmetrical electron and hole configurations participate in these transitions, the energy level notation is common to both charge carriers. For example, by $2eh^1$ we denote two electrons and two holes in their respective first one-carrier energy levels. The vertical lines are numbered in increasing energy order. In this way, different transitions of the same energy are drawn along the same vertical lines. We note that the biexciton binding energy, which amounts to 1.3 meV, is significantly less than the ≈ 7 meV exchange splitting. The various exchange terms, which give rise to the splitting and to the spectral red shifts are also marked in Fig. 3. It is readily seen that optical transitions from a ground level of an odd multiexciton split in a similar way to the splitting discussed in Fig. 2. Starting from the annihilation of the ground state of the fifth multiexciton, both optical transitions split similarly. In addition, the emission spectrum of higher multiexcitons is shifted downward in energy, relative to that of the lower-order ones. The magnitude of this energy shift equals the splitting energy and it can be easily traced back to be the sum of the exchange integrals of all the participating single carrier levels as given in Table I. As a result of these spectral shifts, only two new redshifted spectral lines appear every time that a higher-order ground level of an even multiexciton recom-

binates. In Fig. 4 we present the calculated optical transitions due to the recombination of electrons and holes from the two lowest-lying single carrier energy levels of our infinite potential barrier QD, as a function of the number of excitons within it. Figures 3 and 4 demonstrate the following points. (a) Only two optical transitions are allowed for radiative recombination of an even multiexciton ground state while up to six transitions are allowed for a recombination of an odd multiexciton. (b) The same optical transition can be due to the recombination of up to five different exciton multiplexes. (c) The magnitude of the energy splitting and the spectral redshift for successively higher-order multiexcitons rapidly decrease with the number of excitons, causing the reduction of the transition energy to converge to a finite value. This value can be easily associated with the renormalized band gap of a highly excited bulk semiconductor.¹³ We note here that Fig. 4 describes the case of infinite potential barriers with an infinite number of discrete confined single carrier energy levels. In reality, however, we expect only a very few confined single electron levels before the onset of a spectral continuum.

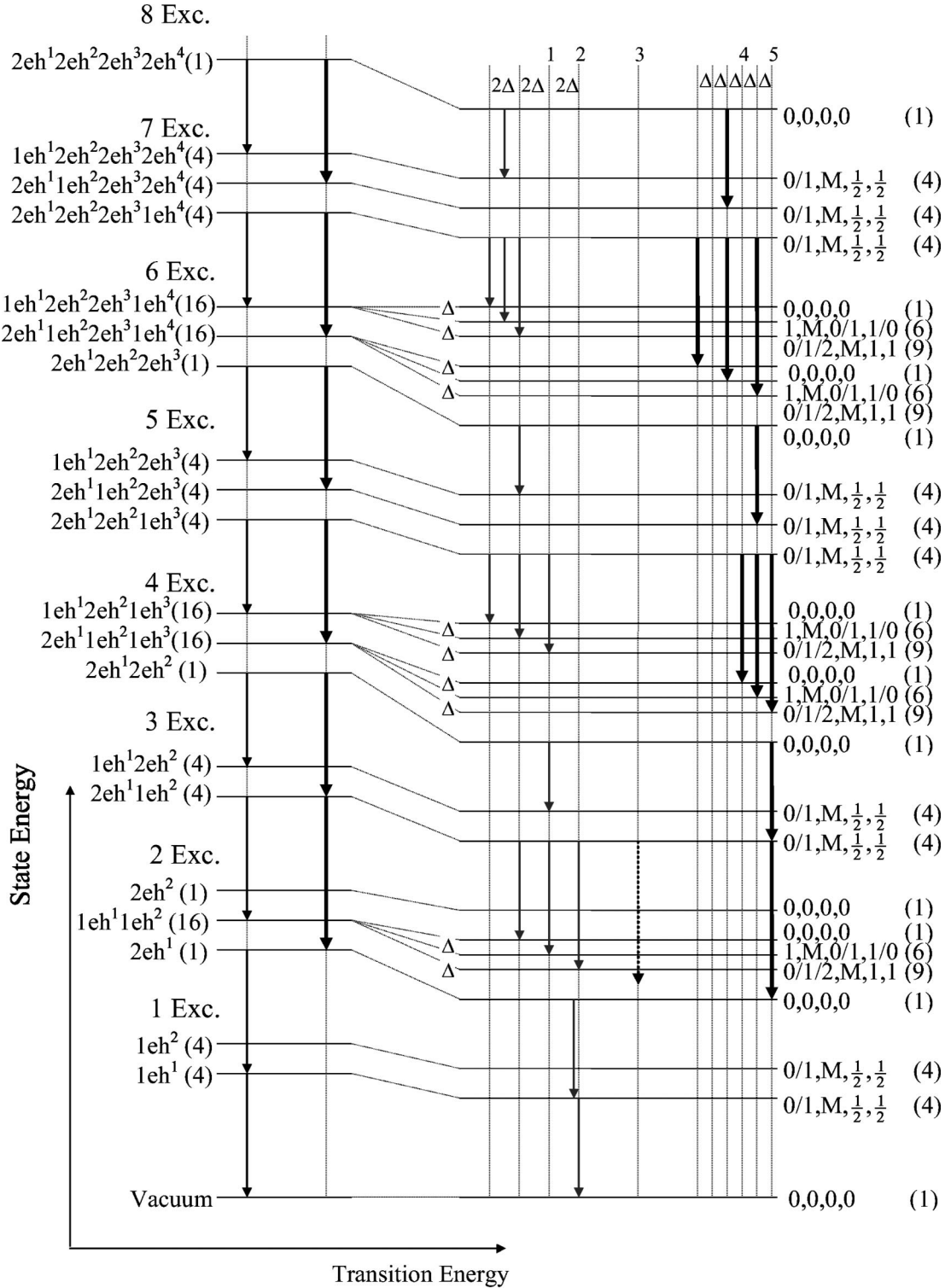


FIG. 3. Schematic description of the allowed optical transitions due to single electron-hole pair annihilation from the ground energy levels of the first eight QD exciton multiplexes. Transitions without (with) consideration of the Coulomb interaction are displayed on the left (right-) hand side. Light gray (thick dark gray) vertical arrows denote the e^1h^1 (e^2h^2) pair recombination. The dashed vertical arrow represents e^2h^1 pair recombination. 2Δ is the sum of electron-electron and hole-hole exchange energies between the first and second single carrier levels.

C. Lifetime of multiexcitons

We assumed so far that the photogenerated multiexcitons thermalize to their ground level much faster than their decay rates. If in addition, we assume that any nonradiative recombination rate is much slower than the radiative ones, then the multiexciton lifetimes can be directly determined from the

calculated optical transitions. The calculated lifetimes for the first few exciton multiplexes in our model quantum dots are presented in Table II.

At any given time, only one well-defined excitonic multiplex may exist in the QD. We define by n_i ($0 < n_i < 1$) the probability of finding the i th excitonic multiplex in the QD.

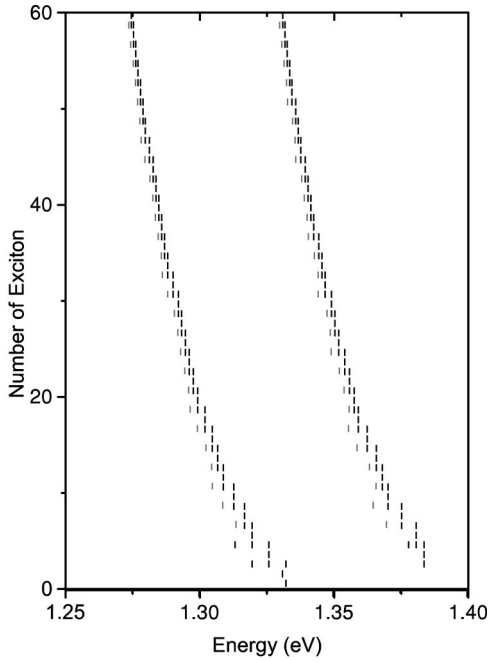


FIG. 4. Vertical bars represent the calculated allowed optical transition energies of increasingly higher QD exciton multiplexes. By light gray vertical bars we denote optical transitions into the upper nondegenerate exchange split states, which due to the lack of degeneracy have smaller intensity.

Thus, for example, n_0 is the probability of finding the QD empty, and n_2 is the probability of finding a biexciton in the QD. We describe the temporal evolution of an exciton multiplex by the following rate equation:

$$\frac{dn_i}{dt} = g_i - \frac{n_i}{\tau_i} + \frac{n_{i+1}}{\tau_{i+1}} - g_{i+1}. \quad (8)$$

Here τ_i is the radiative lifetime of the i th multiexciton and g_i is its photogeneration rate [in Eq. (8), $\tau_0 = \infty$ and $g_0 = 0$]. We note that in addition to the “conventional” first three terms in Eq. (8), there is also a fourth term that describes the decrease in the i th multiexciton occupation probability due to the photogeneration of the $(i+1)$ th multiexciton that causes the i th multiexciton to “vanish.” The photogeneration rate of the i th multiexciton g_i can be expressed as

$$g_i = n_{i-1}G, \quad (9)$$

where $G(t)$ is the total (time dependent) QD exciton photogeneration rate and $G(t)$ is proportional to the power of the external excitation source at a given time. Equation (9) simply expresses the idea that the photogeneration rate of the i th multiexciton depends linearly on the probability that the dot is occupied by the $(i-1)$ th multiexciton. This means, of course, that the QD cannot be emptied by the excitation

TABLE II. Calculated QD multiexciton recombination rates (in units of τ_1^{-1}).

τ_1^{-1}	τ_2^{-1}	τ_3^{-1}	τ_4^{-1}	τ_5^{-1}	τ_6^{-1}	τ_7^{-1}	τ_8^{-1}
1	1.9	13.75	7.21	38.3	15	53.62	20

source (we neglect stimulated emission throughout this analysis). Equation (8) can be analytically solved for both cw and pulse excitations.

III. EXPERIMENTAL RESULTS

A. The sample

The SAQD sample studied here was fabricated by deposition of a coherently strained epitaxial layer of InAs on an $\text{Al}_x\text{Ga}_{1-x}\text{As}$ layer deposited on GaAs substrate. The layer sequence, compositions, and widths are given elsewhere.¹⁴ The SAQD’s were embedded within an $\text{Al}_{0.3}\text{Ga}_{0.7}\text{As}/\text{Al}_{0.1}\text{Ga}_{0.9}\text{As}$ quantum well structure in order to shift the PL emission energy above the silicon band gap. We used sensitive liquid-nitrogen-cooled charge coupled device (CCD) array detector to perform the required very low light level spectroscopy. Note, furthermore, that the $\text{Al}_{0.3}\text{Ga}_{0.7}\text{As}$ barriers prevent vertical diffusion of photogenerated carriers into the SAQD’s. Therefore, the only photons that generate carriers are those absorbed within the quantum wells. The generated carriers then diffuse laterally into the SAQD’s. This allowed a quite accurate estimate of the SAQD photogenerated carrier occupation. Note also that during the growth of the strained layer, the sample was not rotated. Thus a gradient in the QD’s density was formed across its surface. In particular, low-density areas, in which the average distance between neighboring QD’s is larger than our spatial resolution, could easily be found on the sample surface.

B. Experimental setup

We use diffraction-limited low-temperature confocal optical microscope for the PL studies of the single SAQD’s. The setup is schematically described in Fig. 5. We used a $\times 100$ *in situ* microscope objective in order to focus the tunable Ti:sapphire laser light at normal incidence on the sample. Both cw and picosecond pulsed excitations were used. The emitted light was collected by the same microscope objective that was accurately manipulated in three directions using computer-controlled motors. A CCD camera based active feedback loop is used for stabilizing the objective-sample working distance. The collected light was spatially filtered, dispersed by a 0.22 m monochromator and detected by a nitrogen-cooled CCD array detector. The system provides diffraction-limited spatial resolution both in the excitation and the detection channels. We tested the combined spatial resolution of our system by creating selective PL images of a cleaved edge of a single quantum well (SQW) sample.²⁵ The spatial full width at half maximum of the SQW PL emission intensity was found to be 0.5–0.6 μm , in agreement with the expected diffraction-limited optical resolution at this wavelength (≈ 750 nm). The collection efficiency of our system was carefully obtained from the measured spectrum of the reflected laser beam. We found that approximately 3×10^5 photons give rise to one CCD camera count.

C. Photoluminescence line scans and selective wavelength images

The dots position and characteristic emission wavelength are found by taking PL line scans over the SAQD sample

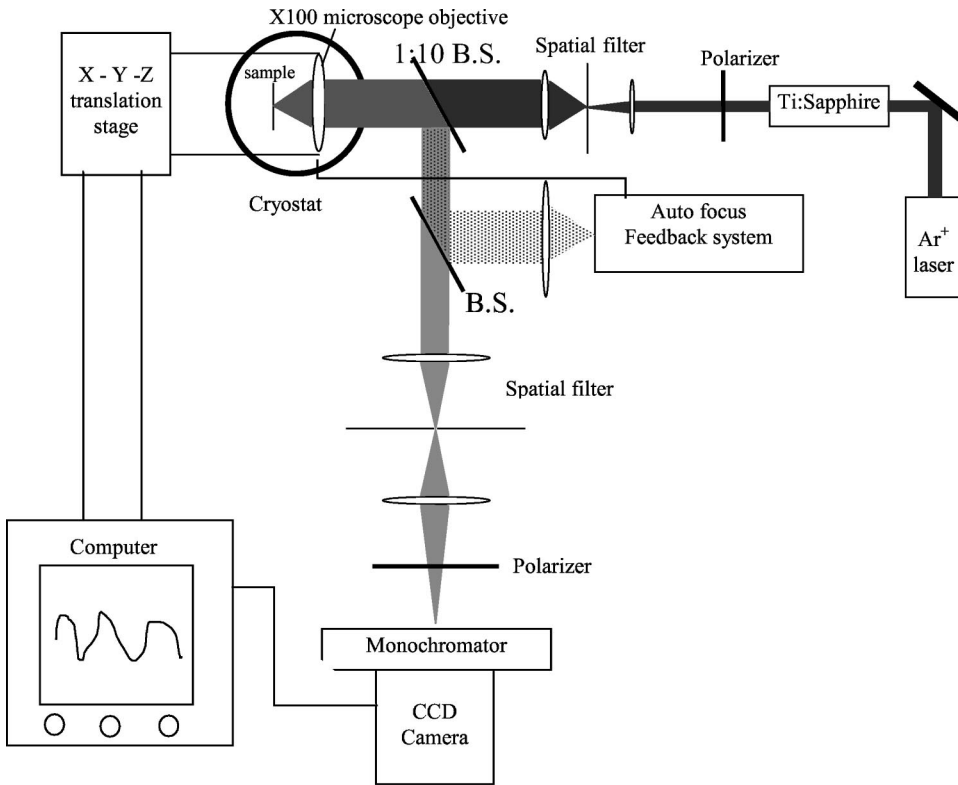


FIG. 5. Schematic description of the low-temperature diffraction-limited confocal microscope setup.

surface. Typical line scans are displayed in Fig. 6, where the PL intensity as a function of photon energy and objective position is given by the gray scale as indicated by the bars in the figures. During the line scan, the PL was excited by $7 \mu\text{W}$ ($30 \mu\text{W}$) of cw, 730-nm laser light, as shown in Figs. 6(a) and 6(b). The microscope objective was moved in steps of $0.1 \mu\text{m}$ [Fig. 6(a)] or $0.25 \mu\text{m}$ [Fig. 6(b)], in each of which the PL spectrum was measured by exposing the CCD camera for 50 s. We note in Fig. 6 that at various positions along the scanned surface, spectrally sharp PL lines are observed. These lines are due to recombination of excitons within single SAQD's, as indicated by their resolution-limited spatial and spectral widths.^{11,15} In the low-power scan, Fig. 6(a), the PL spectrum from each SAQD is mainly composed of a single spectral line. In contrast, however, in the high excitation scan, all the PL spectra contain a few PL lines, which appear in pairs. In order to convince ourselves that, indeed, a single SAQD emits more than one spectral line, we generated selective wavelength images such as those shown in Fig. 7. In Fig. 7 we show four 20×20 selective wavelength images of the sample surface. In order to obtain these images we recorded the full PL spectrum at 400 array points, by exposing the CCD for 10 s at each point. In Fig. 7(a) we present the PL spectrum obtained from one such point, the position of which is marked by the crossing lines on the images of Fig. 7. Four distinct sharp spectral lines are observed in Fig. 7(a). The spectral wavelength of each of these lines was used to generate each one of the images of Fig. 7, respectively, by displaying the intensity of the PL at the selected line wavelength, as a function of the objective position. Inspection of the images clearly demonstrates that each one of the four spectral lines originates from the same

spatial position, and thus conclusively proves that they are emitted from one SAQD. The scanned $6 \mu\text{m} \times 6 \mu\text{m}$ area of Fig. 7 contains a few SAQD's, which we revealed in a similar way (not shown).

Using this procedure, we found that, indeed, the average distance between neighboring SAQD's is larger than our spatial resolution. The PL spectra of each of these SAQD's show several characteristic features. In particular, the sharp spectral lines form one or more groups, and each such group typically contains a pair of particularly strong lines. In general, the number of groups and their PL intensity strongly depends on the power of excitation.

We note here that since the average distance between dots is larger than our spatial resolution and is comparable with the diffusion length, the estimation of the density of the photogenerated carriers within the SAQD can be made quite reliably. One does not have to know the area of the exciting beam for this estimation. In addition, the resonant tunneling structure of our sample¹⁴ prohibits vertical diffusion of carriers, which were generated outside the $\text{Al}_{0.1}\text{Ga}_{0.9}\text{As}$ layer into the SAQD's. From the measured power of the exciting beam and the known index of refraction and absorption of the layers we estimated the carrier generation rate within the SAQD. Thus, using the measured lifetime of photoexcited carriers in similar such SAQD's [0.7 ns (Refs. 26 and 27)] we estimated that with $1 \mu\text{W}$ cw excitation power, three excitons occupy the SAQD on average. Under pulse excitation with the same average power, we obtain over 50 excitons per each laser pulse.

We show below that when nonradiative recombination processes are taken into account, the above estimates are considerably reduced, due to the shortening of the single exciton lifetime.

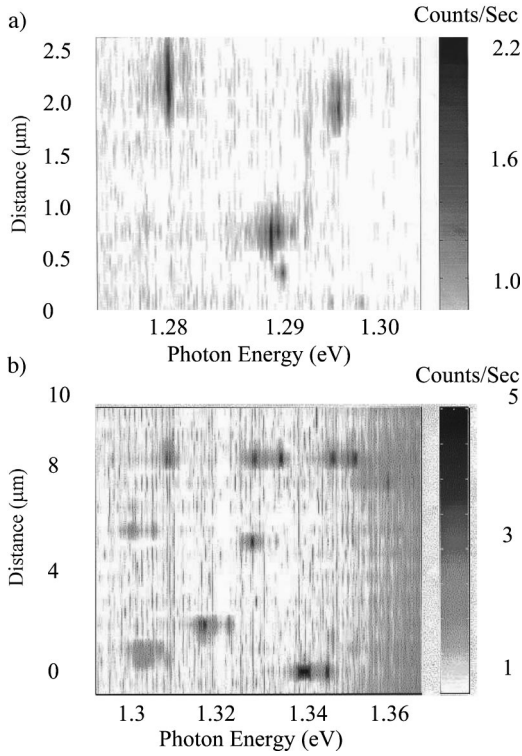


FIG. 6. The PL emission intensity (as indicated by the gray scale) as a function of the photon energy and the microscope position along a line above the sample surface. The sample was excited by a cw laser beam at normal incidence at $7 \mu\text{W}$ (a) and $30 \mu\text{W}$ (b).

D. Power dependence of the PL spectrum of a single SAQD

In Figs. 8 and 9 we present PL spectra from a single SAQD for various excitation powers, using cw and picosecond pulse excitation, respectively. A short horizontal line represents the zero for each spectrum, after subtracting a constant background due to the emission from the GaAs. The PL spectra of both cw and pulsed excitation, which were obtained from two different SAQD's, are composed of two groups of emission lines, with a few characteristic spectral lines in each group. We assigned a serial number to the main lines according to their spectral position. Thus, the lower-energy group is composed of line numbers 1 and 2 and the higher-energy group is composed of line numbers 4 and 5, respectively. Line number 3 is approximately positioned in between the two groups. The energy difference between the groups amounts to 52 meV, while the difference between the pair of lines in each group is approximately 7 meV. These energies are typical for the SAQD PL spectra. Under $1 \mu\text{W}$ cw excitation (Fig. 8) only the lowest-energy PL line number 1 is observed. As the power increases, more spectral lines are observed. At $100 \mu\text{W}$ cw excitation, five main spectral lines are observed. When the excitation power is further increased, two broad spectral bands appear to the lower-energy side of each group of discrete lines. *C1* and *C2* denote these bands, which dominate the PL spectrum for yet higher excitation power. The rate at which the intensity of each emission line grows with the excitation power is different. While the PL intensity of line numbers 2 and 3 saturates for excitation powers of $100 \mu\text{W}$ and $7 \mu\text{W}$, respectively, line number 1 and line number 4 continue to in-

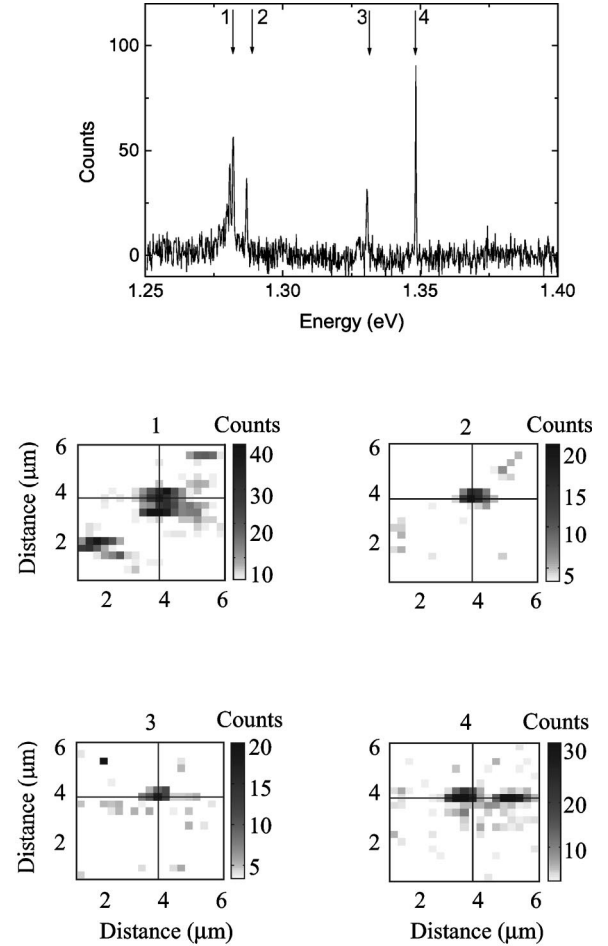


FIG. 7. (a) PL spectrum of a single SAQD. (b) $6 \mu\text{m} \times 6 \mu\text{m}$ selective wavelength images of the sample surface. In each of the images (1 through 4) the intensity of the emitted PL (as indicated by the gray scale) at the energy that corresponds to the spectral line as shown in (a) is displayed as a function of the microscope objective position. The cross on all the images marks the spatial position of the QD.

crease in approximately a square root dependence on the excitation power. They saturate only for excitation powers of over $500 \mu\text{W}$.

There are two main differences between the cw and pulsed excitation as can be seen by comparing Fig. 8 with Fig. 9. First, the total PL intensity under pulse excitation is roughly an order of magnitude lower than that under cw excitation. Second, under pulsed excitation, already at very low excitation power, most of the spectral lines appear.

Finally, it is very important to note that at high excitation power a typical spectral line appears in between line numbers 4 and 5. The significance of this line and its importance in determining the QD symmetry is briefly discussed below.

IV. DISCUSSION

Our experimental findings are analyzed in terms of the theoretical model presented in Sec. II. Although the actual shape of each of the SAQD's that we studied is not known, earlier studies have shown that the base dimensions ($\approx 20\text{--}40 \text{ nm}$) are much larger than its height ($2\text{--}6 \text{ nm}$).⁶ The exact values of the SAQD single carrier energy levels are

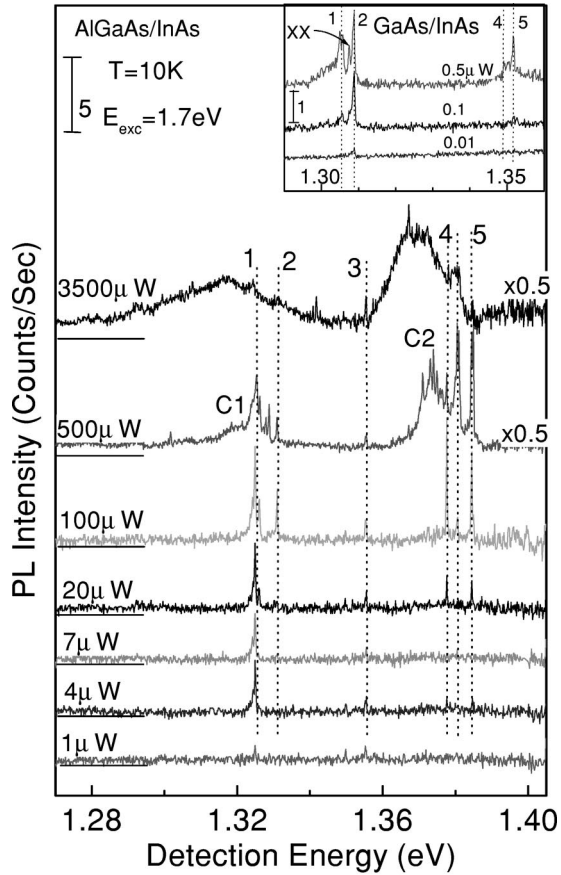


FIG. 8. Single SAQD PL spectra at various cw excitation powers. The spectra are vertically shifted for clarity. The horizontal line to the left of each spectrum marks the corresponding zero emission. The inset contains similar spectra from SAQD sample without aluminum. Note that in this case due to the much less efficient nonradiative decay channels, the single exciton line (number 2) is the first to be observed already at very low excitation powers. The biexciton line (XX) is also observed in these spectra (Ref. 31).

undoubtedly determined by their geometrical shapes, compositions, strain fields, and dimensions.^{28–30} However, these details become of secondary importance for the understanding of the confined multicarrier optical transitions. We have thus chosen a short height, right-angle parallelepiped quantum box of infinite potential in order to calculate the single particle wave functions and energy levels. The advantage of this simplistic description of the QD is that its single carrier energy levels and wave functions can be expressed analytically [Eq. (7)]. We varied the dimensions of our model dot in order to obtain maximum agreement with the measured data. By varying its base dimensions, we mainly affect the energy difference between the single carrier confined levels within the box. We found out that a base dimension of 30 nm gives rise to ≈ 50 meV energy separation between the e^1h^1 single exciton level and the e^2h^2 level. This separation is related to the energy separation between the two main groups of emission lines, which appear in the PL spectra of the SAQD (see Fig. 8). By varying now the third dimension of the box, we mainly affect the Coulomb integrals as given by Eq. (6). The values that we present in Table I were obtained with a box height of 5 nm, which best fitted the characteristic 7-meV splitting between the lines in each group. Finally, we have

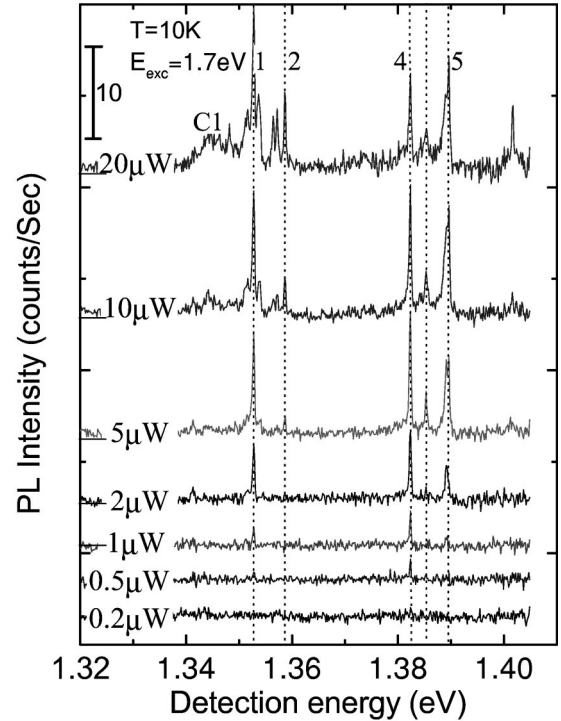


FIG. 9. Single SAQD PL spectrum at various pulse excitation powers. The curves are vertically shifted for clarity. The horizontal line to the left of each spectrum marks the corresponding zero emission.

adjusted the (small) amount by which the base geometrical degeneracy is removed³⁰ by choosing a rectangle base with nearly equal sides. A rectangle side difference of approximately 1 nm, which resulted in 3 meV energy separation between the e^2h^2 and e^3h^3 single carrier states, best accounted for the excitation power dependence of the PL intensity of line numbers 4 and 5, and the line in between them (see Fig. 8). Note that the dimensions that we obtain are very well compared with the reported values.⁶ We stress again that the specific geometry used here is different from that reported in the literature. But since we fit the confined energy level separation, the exchange integral values and the “geometrical degeneracy” to our data, the actual shape of the QD has only a secondary importance.

We proceed by using our rate equation [Eq. (8)] to calculate the emitted PL spectrum as a function of the optical excitation power. We found that at moderate and high excitation powers, our model quite nicely reproduces the measured spectra and their power dependence. At low powers, however, there is a difference between the calculated order by which the spectral lines appear as the excitation power increases and the observed order. While the first observable peak in the experiment is the lowest-energy peak (peak number 1), the model obviously predicts that the first observable peak should have been the single exciton peak, which resides at higher energy (peak number 2). According to the model, only when the number of excitons in the QD exceeds two, the lowest-energy peak (peak number 1) should have appeared. We explain this apparent discrepancy in terms of nonradiative recombination channels that are very efficient at low excitation densities and quickly saturate at higher excitation densities. The nonradiative recombination reveals it-

self in two ways in our experimental measurements. The first is due to the overall count rates that we obtain, which for low power excitation are about two orders of magnitude lower than the expected rates based on PL lifetime measurements³¹ and count rates at higher excitation density. The second is the actual absence of the exciton and biexciton spectral lines in very low density excitations.

Such nonradiative recombination channels are known to be the result of aluminum contained in the layers in which the SAQD's are embedded.³² These nonradiative rates affect the recombination of carriers within the SAQD's.

In order to test this hypothesis, we have measured SAQD samples without aluminum. Few such spectra are depicted for comparison in the inset to Fig. 8. As predicted by our model, in the absence of the nonradiative decay channels associated with the aluminum, the single exciton (line number 2) and biexciton (*XX*) lines are clearly observed in these spectra, already at very low excitation power. Under high excitation power the spectra are quite similar to those presented in Fig. 8. More details on these results will be published elsewhere.³¹ The results are similar to those of Bayer *et al.*¹⁹ who similarly observed the single exciton peaks in the PL emission from SAQD's embedded in aluminum-free layers. The observation of the exciton emission was also reported by other groups.^{8,19} The measurements by Brunner *et al.*⁸ were performed on natural QD's formed by size fluctuation of an $\text{Al}_x\text{Ga}_{1-x}\text{As}/\text{GaAs}$ quantum well. Both exciton and biexciton lines were reported in the emission spectra of these QD's.

Thus, a fast nonradiative decay channel is assumed for the lowest two exciton multiplexes. We then write $1/\tau_{1(2)} = 1/\tau_{1R(2R)} + 1/\tau_{NR}$, where $\tau_{1R(2R)}$ is the radiative lifetime of the exciton (biexciton) ground level and τ_{NR} is their nonradiative lifetime. Since at higher excitation densities our model quite accurately agrees with the measured data, we conclude that the nonradiative lifetime of higher exciton multiplexes is negligible in comparison with their radiative lifetimes. For higher-order multiplexes, saturation and possible screening may make this nonradiative channel ineffective. For example, saturation of nonradiative decay channels such as Shockley-Read-Hall are very well known in bulk semiconductors.³³ Excitation transfer to neighboring dots is yet another nonradiative channel for a single quantum dot (but not necessarily for dot assemblies), which will be saturated just as well at high excitation density. By adjusting the ratio of $\tau_{NR}/\tau_{1R} \approx 0.01$ we successfully obtain the low-power excitation spectra and their power dependence. The results of our calculations are compared in Fig. 10 with the measured PL spectra. We emphasize that the assumption of full thermalization is essential. It is easily verified that without this assumption the emission spectrum is composed of an enormous number of allowed optical transitions, in contrast with the experimental results.

The main difference between the calculated and measured PL spectra is that the latter loses its discrete nature at high excitation power. This is due to the finite number ($\approx 2-5$) of confined electron levels within the "real" SAQD's. Thus, while in our model the exchange energies continue to vary in a discrete manner with the multiexciton order (Figs. 3 and 4), in the real SAQD's it becomes continuous.

Our model qualitatively explains the differences between

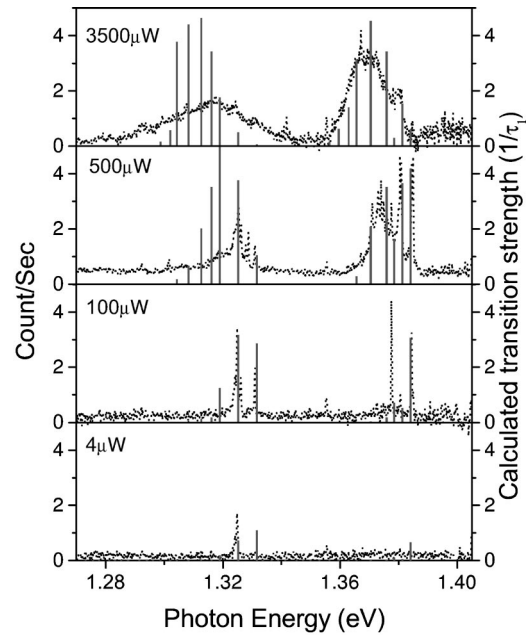


FIG. 10. Comparison between the measured and calculated PL spectra for various cw excitation densities.

the cw and pulsed excitation. In the pulse case the average number of excitons within the SAQD, during the lifetime of the photogenerated carriers, is considerably larger. For that reason, already at very low average power, all the characteristic exciton multiplex lines are observed.

In Fig. 11 we compare the calculated and measured PL intensity of the five spectral lines (1–5) as a function of the photogeneration power. Figures 11(a) and 11(b) represent the cw excitation case, while Figs. 11(c) and 11(d) represent the pulsed excitation case. There is an overall agreement between the measurements and calculations. We note that our model reproduces the evolution of the PL emission with excitation power for both the cw and pulsed cases. Moreover, the absolute emission rates measured at the PL maxima are comparable with our model calculations and the efficiency of our experimental setup. The excitation efficiency at the onset of the emission detection is also comparable with our estimate and the above mentioned nonradiative rates. Inspection of the abscissas of the measured and calculated curves, however, suggests that the number of excitons in the QD is proportional to the square root of the excitation power. Such sublinear dependence may arise from the inefficient diffusion of photogenerated carriers into the SAQD at high excitation densities. It is obvious that at these densities, lateral diffusion of carriers as well as stimulated emission must be correctly taken into account. These processes, however, are beyond the scope of this work.

Comparing the cw and pulsed excitation, and taking into account the repetition rate, we estimate the single exciton radiative lifetime (τ_{1R}) as 3–5 ns. This lifetime completely determines now the effective decay times of the various PL lines. Using our rate equations, we obtain for the various PL lines decay times of 200–700 ps, in agreement with published data obtained by measuring the PL decay time of the SAQD's inhomogeneously broadened spectral line^{26,27} and our more recent time resolved measurements from single QD's.³¹

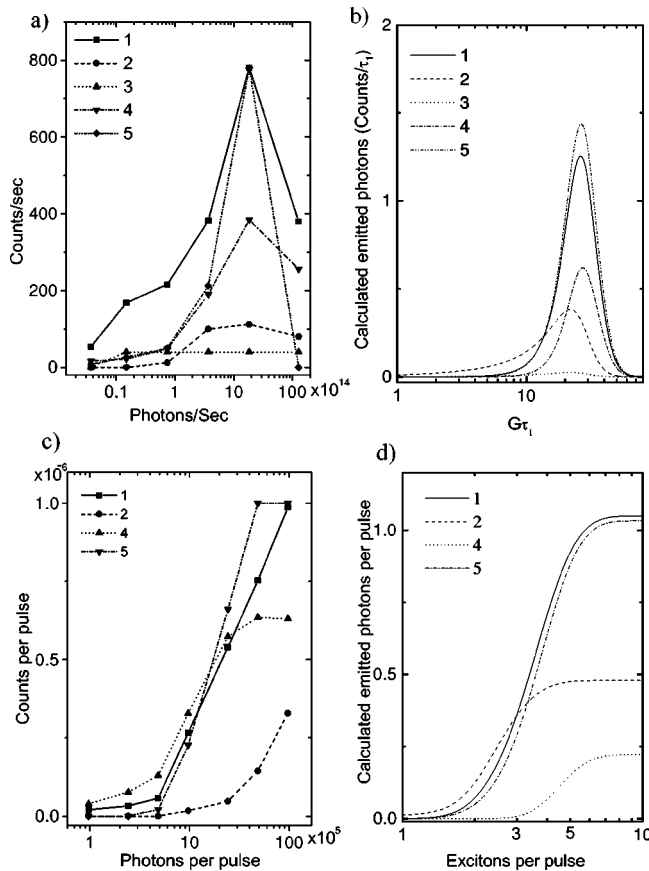


FIG. 11. (a), (b) [(c), (d)] Comparison between the measured and calculated PL intensity of few spectral lines as function of the cw (pulse) excitation power intensity. The line numbers are in accordance with the peak numbers in Fig. 8 (Fig. 9).

V. SUMMARY

We applied low-temperature diffraction-limited confocal optical microscopy to spatially resolve and spectroscopically study photoluminescence emission from single self-assembled semiconductor quantum dots. Using selective wavelength imaging we unambiguously demonstrated that a single photoexcited QD emits light in a few very narrow spectral lines.

In order to explain the measured spectrum and its dependence on the power of either cw or pulsed excitation, we outlined a theoretical many-body model. The model uses analytical single carrier wave functions of a parallelepiped. The Coulomb interaction integrals are then calculated and

used for exact diagonalization of the many-body Hamiltonian, to obtain the many-body eigenenergies and wave functions. The dipole approximation is then used for calculating the oscillator strength for optical transitions between these eigenenergies and their radiative lifetimes.

By adjusting the dimensions of the model parallelepiped we fit the experimentally measured spectra. In addition, we analytically solve the multiexciton radiative rate equations and carefully compare our calculations with the measured data. From this comparison we conclude the following.

(a) The multiline PL spectrum of an optically excited QD is due to optical transitions between confined exciton multiplexes.

(b) A multiexciton relaxes to its ground state much faster than its radiative lifetime. Therefore, at cryogenic temperatures a multiexciton radiatively recombines only from its ground state.

(c) The exchange interaction between single carrier states of the same type reflects itself in the appearance of pairs of lines in the PL spectrum.

(d) With increasing cw excitation power, the emission intensity of the spectral lines reaches maximum and then starts to decrease, while new spectrally redshifted lines appear. The new lines similarly depend on the excitation power.

(e) The spectral redshifts of the new lines are due to the exchange energy between single carrier levels of increasing energy. Once the discrete levels of the QD are fully occupied, spectrally broad bands are formed due to transitions involving continuum electronic states.

(f) The order by which the spectral lines appear and reach their maximum as the excitation power gradually increases yields information about the symmetry of the QD. We show that the self-assembled quantum dots that we investigated have only spin degeneracy but no geometrical degeneracy.

(g) Efficient nonradiative decay channels determine the recombination times of single excitons in SAQD's embedded in Al containing layers. Therefore, the actual measured PL decay times at low excitation density are much shorter than the single exciton radiative lifetime that we found here to be a few nanoseconds long.

ACKNOWLEDGMENTS

The research was supported by the U.S.-Israel Binational Science Foundation (453/97) and the Technion Fund for the promotion of research.

¹D. Bimberg, M. Grundmann, and N. N. Ledentsov, *Quantum Dot Heterostructures* (Wiley, New York, 1998).

²I.N. Stranski and L. Krastanow, *Akad. Wiss. Lit. Mainz Abh. Math. Naturwiss. Kl.* **146**, 767 (1939).

³J.Y. Marzin, J.M. Gerard, A. Israel, D. Barrier, and G. Bastard, *Phys. Rev. Lett.* **73**, 716 (1994).

⁴H. Drexler, D. Leonard, W. Hansen, J.P. Kotthaus, and P.M. Petroff, *Phys. Rev. Lett.* **73**, 2252 (1994).

⁵S. Fafand, R. Leon, D. Leonard, J. L. Merz, and P. M. Petroff, *Phys. Rev. B* **50**, 8086 (1994).

⁶D. Leonard, K. Pond, and P.M. Petroff, *Phys. Rev. B* **50**, 11 687 (1994).

⁷R. Heitz, A. Kalburge, Q. Xie, M. Grundmann, P. Chen, A. Hoffmann, A. Madhukar, and D. Bimberg, *Phys. Rev. B* **57**, 9050 (1998).

⁸K. Brunner, G. Abstreiter, G. Bohm, G. Trankle, and G. Weimann, *Phys. Rev. Lett.* **73**, 1138 (1994).

⁹H. Kamada, H. Ando, J. Temmyo, and T. Tamamura, *Phys. Rev. B* **58**, 16 243 (1998).

- ¹⁰Y. Toda, S. Shinomori, K. Suzuki, and Y. Arakawa, *Phys. Rev. B* **58**, 10 147 (1998).
- ¹¹D. Gammon, E.S. Snow, B.V. Shanabrook, D.S. Katzer, and D. Park, *Phys. Rev. Lett.* **76**, 3005 (1996).
- ¹²A. Barenco and M.A. Dupertuis, *Phys. Rev. B* **52**, 2766 (1995).
- ¹³A. Wojs and P. Hawrylak, *Phys. Rev. B* **55**, 13 066 (1997).
- ¹⁴E. Dekel, D. Gershoni, E. Ehrenfreund, D. Spektor, J.M. Garcia, and P.M. Petroff, *Phys. Rev. Lett.* **80**, 4991 (1998).
- ¹⁵H.F. Hess, E. Betzig, T.D. Harris, L.N. Pfeiffer, and K.W. West, *Science* **264**, 1740 (1994).
- ¹⁶N.H. Bonadeo, G. Chen, D. Gammon, D.S. Katzer, D. Park, and D.G. Steel, *Phys. Rev. Lett.* **81**, 2759 (1998).
- ¹⁷W. Heller, U. Bockelmann, and G. Abstreiter, *Phys. Rev. B* **57**, 6270 (1998).
- ¹⁸U. Bockelmann, W. Heller, and G. Abstreiter, *Phys. Rev. B* **55**, 4469 (1997).
- ¹⁹M. Bayer, T. Gutbrod, A. Forchel, V.D. Kulakovskii, A. Gorbunov, M. Michel, R. Steffen, and K.H. Wang, *Phys. Rev. B* **58**, 4740 (1998).
- ²⁰M. Ikezawa, Y. Masumoto, T. Takagahara, and S.V. Nair, *Phys. Rev. Lett.* **79**, 3522 (1997).
- ²¹L. Landin, M.S. Miller, M.E. Pistol, C.E. Pryor, and L. Samuelson, *Science* **280**, 262 (1998).
- ²²A. Franceschetti, L.W. Wang, H. Fu, and A. Zunger, *Phys. Rev. B* **58**, 13 367 (1998).
- ²³M. Nirmal *et al.*, *Phys. Rev. Lett.* **75**, 3728 (1995).
- ²⁴S. Adachi, *J. Appl. Phys.* **58**, R1 (1985).
- ²⁵T.D. Harris, D. Gershoni, R.D. Grober, L.N. Pfeiffer, K.W. West, and N. Chand, *Appl. Phys. Lett.* **68**, 988 (1996).
- ²⁶S. Grosse, J.H.H. Sandmann, G. von Plessen, J. Feldmann, H. Lipsanen, M. Sopanen, J. Tulkki, and J. Ahopelto, *Phys. Rev. B* **55**, 4473 (1997).
- ²⁷M. Bresken, M. Lindberg, M. Sopanen, H. Lipsanen, and J. Tulkki, *Phys. Rev. B* **58**, 15 993 (1998); **55**, 4477 (1997).
- ²⁸M. Grundmann, O. Stier, and D. Bimberg, *Phys. Rev. B* **52**, 11 969 (1995).
- ²⁹C.E. Pryor, M.-E. Pistol, and L. Samuelson, *Phys. Rev. B* **56**, 10 404 (1997).
- ³⁰J. Kim, L.W. Wang, and A. Zunger, *Phys. Rev. B* **57**, 9408 (1998).
- ³¹E. Dekel, D. Regelman, D. Gershoni, E. Ehrenfreund, W.V. Schoenfeld, and P.M. Petroff (unpublished).
- ³²I. Shtrichman, D. Gershoni, and R. Kalish, *Phys. Rev. B* **56**, 1509 (1997).
- ³³R. K. Ahrenkiel, in *Semiconductors and Semimetals*, edited by R. K. Ahrenkiel and M. S. Lundstrom (Academic, San Diego, 1993), Vol. 39.